Content Based Image Retrieval Using Depth Maps for Colonoscopy Images

Md Marufi Rahman[1][a], JungHwan Oh[1][b], Wallapak Tavanapong[2] and Piet C. de Groen[3]
[1]*Dept. of Comp. Sci. and Eng., University of North Texas, Denton, TX 76203, U.S.A.*
[2]*Computer Science Department, Iowa State University, Ames, IA 50011, U.S.A.*
[3]*Division of Gastroenterology Hepatology and Nutrition, University of Minnesota, MN 55455, U.S.A.*

Keywords: CBIR, Deep Learning, Depth Map, Colonoscopy, Vision Transformer (ViT).

Abstract: Content Based Image Retrieval (CBIR) finds similar images given a query image. Effective CBIR has been actively studied over several decades. For measuring image similarity, low-level visual features (i.e., color, shape, texture, and spatial layout), combination of low-level features, or Convolutional Neural Network (CNN) are typically used. However, a similarity measure based on these features is not effective for some type of images, for example, colonoscopy images captured from colonoscopy procedures. This is because the low-level visual features of these images are mostly very similar. We propose a new method to compare these images and find their similarity in terms of their surface topology. First, we generate a grey-scale depth map image for each image, then extract four straight lines from it. Each point in the four lines has a grey-scale value (depth) in its depth map. The similarity of the two images is measured by comparing the depth values on the four corresponding lines from the two images. We propose a function to compute a difference (distance) between two sets of four lines using Mean Absolute Error. The experiments based on synthetic and real colonoscopy images show that the proposed method is promising.

1 INTRODUCTION

QBE (Query by Example) is a query method in CBIR (Content Based Image Retrieval) in which a query image is compared with the images in a database, and several most similar images are retrieved as a result (Meenalochini et al., 2018; Öztürk et al., 2021; Chen et al., 2021). The underlying comparison algorithms may vary depending on the application but result images should have common elements with the given query image. These comparison algorithms use low-level visual features (i.e., color, shape, texture, and spatial layout), low-level feature fusion, local feature (sparse representation), or Convolutional Neural Network (CNN) (Latif et al., 2019). However, we found that the aforementioned features are not effective for similarity comparisons for some type of images (see Figure 1(a) and Figure 3). These images are from colonoscopy videos (Mokter et al., 2022; Rahman et al., 2021; Mokter et al., 2020; Tejaswini et al., 2019), in which low-level visual features (i.e., color, shape, texture, and spatial layout) are very similar. Therefore, we define the similarity among this type of images in terms of their surface topology. For example, all images in Figure 3 are similar in terms of their surface topology.

In this paper, we propose a new method to compare these images and find their similarity (in term of their surface topology). First, we generate a grey-scale depth map image (Ranftl et al., 2021 – more details can found in Section 3.1) for each image (see Figure 1. (b)), then extract four straight lines: Horizontal Line (called Blue line), Vertical Line (called Green line), Primary Diagonal Line (called Orange line), and Secondary Diagonal Line (called Red line). Given a depth map image, the dark areas in the image are closer to the camera and the bright areas are relatively further from the camera.

Each point in the four lines has a grey-scale value in its depth map. If we plot the four lines into two-dimensional space such that the x-axis is a position of each point in the line, and the y-axis is a grey-scale

[a] https://orcid.org/0000-0001-8402-420X
[b] https://orcid.org/0000-0001-5173-6788

Rahman, M., Oh, J., Tavanapong, W. and C. de Groen, P.
Content Based Image Retrieval Using Depth Maps for Colonoscopy Images.
DOI: 10.5220/0011749100003414
In *Proceedings of the 16th International Joint Conference on Biomedical Engineering Systems and Technologies (BIOSTEC 2023) - Volume 4: BIOSIGNALS*, pages 301-308
ISBN: 978-989-758-631-6; ISSN: 2184-4305

value of each point in the line, its result can be seen in Figure 1(c). A comparison between two given images, Image *A* and Image *B* can be a comparison between the four lines from Image *A* and the four lines from Image *B*. We also propose a function to compute a difference (distance) between a set of four lines from one image and that from the other image using Mean Absolute Error (MAE) (Willmott et al., 2005) (details in section 3.2). By applying this distance function to a pair of images, we can find most similar images for a given query image.

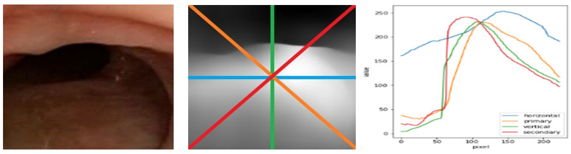

(a) (b) (c)

Figure 1: (a) Original color image, (b) Its depth map with four lines (Blue: Horizontal Line, Green: Vertical Line, Orange: Primary Diagonal Line, and Red: Secondary Diagonal Line), and (c) Grey-scale value plots for the four-lines.

The main contributions of this work are as follows. First, we propose to use depth maps for an image comparison for the first time to the best of our knowledge. Second, we propose a function to compare two depth maps very effective for the first time as far as we know. The rest of the paper is organized as follows. Section 2 discusses the related work. Section 3 describes the proposed methodology. Section 4 shows our experimental results. Finally, Section 5 summarizes our concluding remarks.

2 RELATED WORK

In this section we provide a brief overview of recent studies about depth estimation. We use the result of these studies in our technique.

Almost all existing architectures for depth estimation are based on convolutional architectures with an encoder and a decoder. Encoders progressively downsample the input image to extract features at multiple scales. However, downsampling has distinct drawbacks that are particularly salient in depth estimation tasks. That is feature resolution and granularity are lost in the deeper stages of the model and can thus be hard to recover in the decoder (Ranftl et al., 2021). Instead of using the downsampling, the authors of (Ranftl et al., 2021) proposed to use vision transformer (ViT) which foregoes explicit downsampling operations after an initial image embedding has been computed and maintains a representation with constant dimensionality throughout all processing stages. They reported a performance increase of more than 28% when compared to the top-performing fully-convolutional network on the various datasets.

A conditional generative adversarial network, Pix2pix based method was proposed to transform monocular endoscopic image to depth map (Rau et al., 2019). To overcome the lack of labelled training data in endoscopy, the authors proposed to use simulation environments and to additionally train the generator and discriminator of the model on unlabelled real video frames in order to adapt to real colonoscopy environments. They reported promising results on synthetic, phantom and real datasets and showed that generative models outperform discriminative models when generating depth maps from colonoscopy images, in terms of both accuracy and robustness.

A method using DenseNet-169 was proposed in (Alhashim & Wonka, 2018) to generate a high-resolution depth map given a single RGB color image with the help of transfer learning. Following the standard encoder-decoder architecture, the authors leverage features extracted using high performing pre-trained networks when initializing their encoder along with augmentation and training strategies that lead to more accurate results. They reported that the proposed method with fewer parameters and training iterations, outperformed the other two methods (Laina et al., 2016; Fu et al., 2018) on two datasets.

We used these three approaches discussed above to generate depth maps for the proposed work. For convenience, we call the approach in (Ranftl et al., 2021) as 'MiDas', the approach in (Rau et al., 2019) as 'Pix2pix', and the approach in (Alhashim & Wonka, 2018) as 'DenseNet-169'.

3 PROPOSED METHOD

We discuss Depth map generation, feature extraction, and comparison in this section.

3.1 Depth Map Generation

For MiDas we used the code from the web page (https://github.com/isl-org/dpt) provided in (Ranftl et al., 2021). We implemented the code with Python 3.7, PyTorch 1.8.0, OpenCV 4.5.1, and PyTorch Image Models (timm 0.4.5) per the webpage (https://github.com/isl-org/dpt). We generated depth map of our input image by calling the monocular depth estimation model.

For Pix2pix we used code from TensorFlow GitHub page which cites the original paper (Isola et al., 2017) for the implementation (https://www.tensorflow.org/tutorials/generative/Pix2pix). For DenseNet-169 we used code from the web page (https://github.com/ialhashim/DenseDepth) provided in (Alhashim & Wonka, 2018).

To generate depth maps using Pix2pix and DenseNet-169, we needed to train them using a relevant data while MiDas does not need any training. We used the dataset in (http://cmic.cs.ucl.ac.uk/ColonoscopyDepth/) provided in (Rau et al., 2019). This dataset has 16,016 synthetic colonoscopy images with their corresponding ground truth depth map images. We split these images to training samples: 10,346, validation samples: 4,435, and testing samples: 1,235. We used these three methods (MiDas, Pix2pix, DenseNet-169) to generate depth map images for the experiments, and their performance comparison is reported in Section 4.

3.2 Feature Extraction and Depth Map Comparison

To compare depth map images, four straight lines are extracted as discussed before (see Figure 1). Each point in the four lines has a grey-scale value in its depth map. Assume that a given image, A is a square size of S (width) × S (height) pixels in which its width and height are same. It consists of S^2 pixels in which a pixel is denoted as p_{ij} where i is a row number and j is a column number. Horizontal Line (*HL*), Vertical Line (*VL*), Primary Diagonal Line (*PL*), and Secondary Diagonal Line (*SL*) of an image A are defined as follows.

$$HL_A = \{p^A{}_{ij}\} \text{ where } i = \left\lceil \frac{S}{2} \right\rceil, j = 1, 2, \ldots S \tag{1}$$

$$VL_A = \{p^A{}_{ij}\} \text{ where } i = 1, 2, \ldots S, j = \left\lceil \frac{S}{2} \right\rceil \tag{2}$$

$$PL_A = \{p^A{}_{11}, p^A{}_{22},\ p^A{}_{33},\ \ldots\ p^A{}_{SS}\} \tag{3}$$

and

$$SL_A = \{p^A{}_{1S}, p^A{}_{2(S\text{-}1)},\ p^A{}_{3(S\text{-}2)},\ \ldots\ p^A{}_{S1}\} \tag{4}$$

All the four lines have the same number of pixels, which are used to derive features to represent a given image.

A comparison between two given images, Image *A* and Image *B* can be a comparison between the four lines from Image *A* and the four corresponding lines from Image *B*. A difference (distance) between Image *A* and Image *B*, D_{AB} can be calculated using Mean Absolute Error (MAE) (Willmott et al., 2005) and defined as follows.

$$D_{AB}^{MAE} = \frac{1}{S} \times ((HL_A - HL_B) + (VL_A - VL_B) + (PL_A - PL_B) + (SL_A - SL_B)) \tag{5}$$

where,

$$HL_A - HL_B = |p^A{}_{ij} - p^B{}_{ij}| \text{ where } i = \left\lceil \frac{S}{2} \right\rceil,\ j = 1, 2, \ldots S \tag{6}$$

$$VL_A - VL_B = |p^A{}_{ij} - p^B{}_{ij}| \text{ where } i = 1, 2, \ldots S, j = \left\lceil \frac{S}{2} \right\rceil \tag{7}$$

$$\begin{aligned} PL_A - PL_B = {} & |p^A{}_{11} - p^B{}_{11}| + |p^A{}_{22} - p^B{}_{22}| \\ & + |p^A{}_{33} - p^B{}_{33}| + \ldots + |p^A{}_{SS} - p^B{}_{SS}| \end{aligned} \tag{8}$$

$$\begin{aligned} SL_A - SL_B = {} & |p^A{}_{1S} - p^B{}_{1S}| + |p^A{}_{2(S\text{-}1)} - p^B{}_{2(S\text{-}1)}| \\ & + |p^A{}_{3(S\text{-}2)} - p^B{}_{3(S\text{-}2)}| + \ldots + |p^A{}_{S1} - p^B{}_{S1}| \end{aligned} \tag{9}$$

Choosing an effective comparison method to measure the difference (distance) between the two sets of the four lines is challenging. We tested several different methods (see Equations (5), (10) – (12) below) to calculate the difference (distance). Equation (10) is using Root Mean Square Error (RMSE - Willmott et al., 2005). Equation (11) called Metric1 is calculating absolute differences between the first derivatives of the feature lines (Equations (1), (2), (3), (4)), and taking a summation of those differences. Equation (12) called Metric2 is calculating a difference (distance) in the same way as Equation (11), using the second derivatives instead. Among them, MAE in Equation (5) provided a better accuracy (i.e., F1 score) compared to the others. More details can be found in Section 4.4.

$$D_{AB}^{RMSE} = \sqrt[2]{\frac{1}{S} \times ((HL_A - HL_B)^2 + (VL_A - VL_B)^2 + (PL_A - PL_B)^2 + (SL_A - SL_B)^2} \tag{10}$$

$$\begin{aligned} D_{AB}^{Metric1} = {} & \left|\frac{d}{dx}(HL_A) - \frac{d}{dx}(HL_B)\right| + \left|\frac{d}{dx}(VL_A) - \frac{d}{dx}(VL_B)\right| + \left|\frac{d}{dx}(PL_A) - \frac{d}{dx}(PL_B)\right| \\ & + \left|\frac{d}{dx}(SL_A) - \frac{d}{dx}(SL_B)\right| \end{aligned} \tag{11}$$

$$\begin{aligned} D_{AB}^{Metric2} = {} & \left|\frac{d^2}{dx^2}(HL_A) - \frac{d^2}{dx^2}(HL_B)\right| + \left|\frac{d^2}{dx^2}(VL_A) - \frac{d^2}{dx^2}(VL_B)\right| \\ & + \left|\frac{d^2}{dx^2}(PL_A) - \frac{d^2}{dx^2}(PL_B)\right| + \left|\frac{d^2}{dx^2}(SL_A) - \frac{d^2}{dx^2}(SL_B)\right| \end{aligned} \tag{12}$$

4 EXPERIMENTS AND RESULTS

In this section we discuss the datasets used for the experiments, an accuracy comparison of the three depth map generation methods discussed in Section 3, and a performance evaluation of the proposed feature extraction with deep learning-based feature extraction method. We used a workstation with Intel(R) Core (TM) i7–10700 CPU @ 2.9 GHz 8 Core(s), 16 Logical Processor(s), and NVIDIA Geforce RTX 2070 Super with 8GB RAM for our experiments.

4.1 Datasets

We used two datasets for the experiments. The first dataset (Rau et al., 2019) has 16,016 synthetic colonoscopy images with their corresponding ground truth depth map images. More details of the dataset can be found in the paper (Rau et al., 2019) as mentioned in Section 3.1. From this dataset, we selected 200 images in which there are 20 groups with 10 images per group. For convenience, we call it Dataset1. All images in one group are all similar in term of their contents (i.e., their surface topology). Figure 2 shows five similar images of one group in this dataset. The resolution of each image is 256 × 256 pixels.

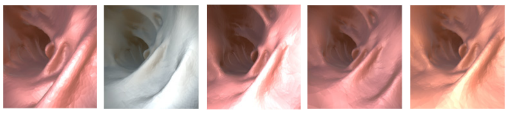

Figure 2: Five similar images in one group from Dataset1.

The second dataset has 140 real colonoscopy images which was used in our previous work (Author1; Author2; Author3; Author4; Author5; Author6). For this dataset, we selected 140 images from 140 colonoscopy procedures to create a more practical and challenging dataset, in which there are 28 groups with 5 images per group. For convenience, we call it Dataset2. All images in one group are all similar in terms of their contents (i.e., their surface topology). Figure 3 shows five images of one group in this dataset. The resolution of each image is 224 × 224 pixels. Table 1 summarizes these two datasets.

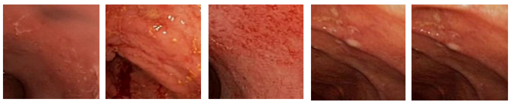

Figure 3: Five similar images in one group from Dataset2.

Table 1: Dataset details.

Dataset type	No. of Images	No. of groups	No. of frames per groups
Synthetic colonoscopy image (Dataset1)	200	20	10
Real colonoscopy image (Dataset2)	140	28	5

4.2 Depth Map Generation

The dataset of the synthetic colonoscopy images already has their corresponding ground truth depth map images. However, the dataset with the real colonoscopy images does not have any depth map, so we need to generate them. We discussed the three methods generating depth maps in Section 3.1. Here, we compared the performance of these methods to find the best method. First, we applied the three methods to the synthetic colonoscopy images in Dataset1 and generated their corresponding depth map images. And the generated depth maps were compared with the corresponding ground truth depth map images using Root Mean Square Error (RMSE) as follows.

$$RMSE = \sqrt{\frac{1}{MxN}\sum_{i=0,j=0}^{M-1,N-1}[I(i,j)-K(i,j)]^2} \qquad (13)$$

where I and K are two images to be compared, the resolution of each image is M (width) x N (height) pixels. RMSE is a square root of an average of pixel differences in the same position. Its value is always non-negative, and a value closed to zero indicates that two images are very similar. We calculated a mean RMSE value for all 200 images in Dataset1. We did this testing for Dataset1 since Dataset2 does not have any ground truth depth map images, so there is nothing to be compared.

Table 2 shows that the mean RMSE values from the three depth map generation methods are very close to zero, which indicates all the methods provide reasonable accuracies. The mean RMSE value of MiDas is a bit larger than those of the other two methods. These two methods (Pix2pix and DenseNet-169) were trained using Dataset1 and tested with 200 images (not used for training) in Dataset1. Pix2pix and DenseNet-169 are more accurate since the training and testing images are from the same synthetic image dataset, but MiDas was not trained using any dataset since its structure does not need any training.

Table 2: Comparison of three depth map generation methods with their mean RMSE values using Dataset1.

Depth Map method	Mean RMSE value
MiDas	0.030345
Pix2pix	0.012239
DenseNet-169	0.016127

4.3 Feature Extraction and Comparison Examples

In this section, we show some examples about the feature extraction and comparison discussed in Section 3.2. The two synthetic images from Dataset1 in Figure 4(a) and (b) are very similar in terms of their surface topology even if they are different in terms of their colors. The image in Figure 4(c) is not similar with them. Figure 4(d), (e) and (f) show their corresponding ground truth depth maps and four lines. Figure 4(g), (h) and (i) are showing their corresponding grey-scale value plots for the four-lines. The difference (distance) between the two images in Figure 4(a) and (b) using Equation (5) is 24.39. The same difference (distance) between the two images in Figure 4(a) and (c) using Equation (5) is 85.14. This means that Figure 4(a) is relatively more similar with Figure 4(b), but it is less similar with Figure 4(c).

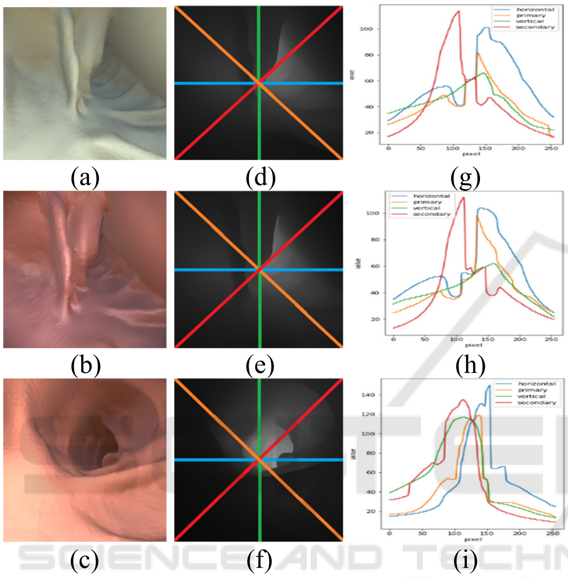

Figure 4: (a), (b) (c): Original Color Images from Dataset1, (d), (e), (f) Corresponding depth maps with four lines, and (g), (h), (i): Corresponding Grey-scale value plots for the four-lines.

The two real Colonoscopy images from Dataset2 in Figure 5(a) and (b) are very similar in term of their surface topology. The image in Figure 5(c) is not similar with them. Figure 5(d), (e) and (f) show their corresponding depth maps and four lines. These depth maps were generated using MiDas. Figure 5(g), (h) and (i) show their corresponding grey-scale value plots for the four-lines. The difference (distance) between the two images in Figure 5(a) and (b) using Equation (5) is 78.08. The same difference (distance) between the two images in Figure 5(a) and (c) using Equation (5) is 411.60. This means that Figure 5(a) is relatively more similar with Figure 5(b), but it is less similar with Figure 5(c).

4.4 Depth Map Comparison Results

For a comprehensive comparison, we compared our proposed feature-based method with a deep learning based CBIR method. In this method, Resnet50 (He et al., 2016) was used as a feature extractor. This feature extractor collects a feature vector of 1,024 dimensions for each image. Euclidian distance was used to calculate a similarity between the feature vectors of images.

These two methods (Proposed feature-based and Resnet50 feature-based) were applied to the different Image sets such as the ground truth depth maps of Dataset1, the depth maps generated using the three depth map generation methods in Section 3.1 applied to Dataset2, and the original color images from Dataset1 and Dataset2. We included the original color images from Dataset1 and Dataset2 for a fair and comprehensive comparison with the Resnet50 based method. All these cases are summarized in Table 3 below. For convenience, we call the proposed feature based method as DepthSim (DS), and the Resnet 50 feature based method as Resnet50 (R50).

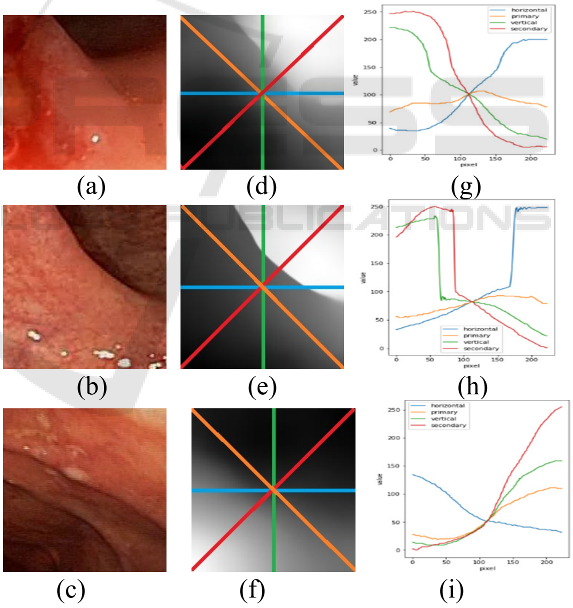

Figure 5: (a), (b) (c): Original Color Images from Dataset1, (d), (e), (f) Corresponding depth maps with four lines, and (g), (h), (i): Corresponding Grey-scale value plots for the four-lines.

We report the F1 score (Alsmadi et al., 2017) since it is a combination of Precision and Recall, which are defined as follows. A high F1 score value is desirable.

For both Dataset1 and Dataset2, we tested four different query types (Top1, Top2, Top3 and Top4). Top1 means a single most similar image is retrieved using the corresponding method, and we check if it is similar with the given query image, in other words, if it is in the same group of the query image. Similarly, Top2, Top3 and Top4 mean most similar two, three and four images are retrieved, and we check if they are in the same group of the query image.

Table 3: All cases for two methods applied to Dataset1 and Dataset2.

Cases	Methods	Images used
Case 1 (DS-Dep-D1)	DepthSim (DS)	Ground truth Depth maps in Dataset1
Case 2 (R50-Dep-D1)	Resnet50 (R50)	Ground truth Depth maps in Dataset1
Case 3 (DS-RGB-D1)	DepthSim (DS)	Original color Images in Dataset1
Case 4 (R50-RGB-D1)	Resnet50 (R50)	Original color Images in Dataset1
Case 5 (DS-MiDas-D2)	DepthSim (DS)	Depth maps by MiDas for Dataset2
Case 6 (R50-MiDas-D2)	Resnet50 (R50)	Depth maps by MiDas for Dataset2
Case 7 (DS-DenseNet-D2)	DepthSim (DS)	Depth maps by DenseNet-169 for Dataset2
Case 8 (R50-DenseNet-D2)	Resnet50 (R50)	Depth maps by DenseNet-169 for Dataset2
Case 9 (DS-Pix2pix-D2)	DepthSim (DS)	Depth maps by Pix2pix for Dataset2
Case 10 (R50-Pix2pix-D2)	Resnet50 (R50)	Depth maps by Pix2pix for Dataset2
Case 11 (DS-RGB-D2)	DepthSim (DS)	Original color Images in Dataset2
Case 12 (R50-RGB-D2)	Resnet50 (R50)	Original color Images in Dataset2

$$Recall = \frac{\textit{number of similar images retrieved}}{\textit{total number of similar images in database}} \qquad (14)$$

$$Precision = \frac{\textit{number of similar images retrieved}}{\textit{total number of images retrieved}} \qquad (15)$$

$$F1\ score = \frac{2 \times (precision \times recall)}{precision + recall} \qquad (16)$$

Table 4 shows F1 scores for Case1 (DS-Dep-D1) through Case 4 (R50-RGB-D1) in Table 3, and indicates the proposed feature-based method performs better than Resnet50 feature-based method for all different image sets from Dataset1. As seen in Table 4, the proposed method achieves around 86.8 ~ 92.5 % of accuracy on the ground truth depth map images from Dataset1.

Table 4: Two methods and their accuracies of four different retrievals on Dataset1.

Experiment	Top1	Top2	Top3	Top4
Case 1 (DS-Dep-D1)	**0.925**	**0.905**	**0.883**	**0.868**
Case 2 (R50-Dep-D1)	0.855	0.793	0.742	0.705
Case 3 (DS-RGB-D1)	0.695	0.633	0.567	0.524
Case 4 (R50-RGB-D1)	0.520	0.450	0.401	0.368

Figure 6 shows an example of a query image (Figure 6(a) from Dataset1) and the retrieved images (Figure 6(b), (c), (d) and (e)) using the proposed method. They are all very similar in terms of surface topology regardless of their colors.

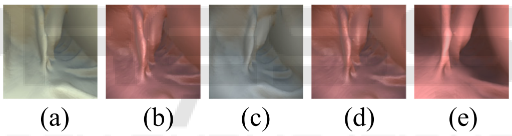

Figure 6: (a) query image, (b), (c), (d), and (e) retrieved images based on the proposed method.

Figure 7 shows an example of a query image and retrieved images. Figure 7(a) is the query image (same image in Figure 6 (a)), and Figure 7(b), (c), (d) and (e) are retrieved images using the Resnet50 based method. Only Figure 7 (c) is similar with the query (Figure 7 (a)). All others are not very similar in terms of surface topology.

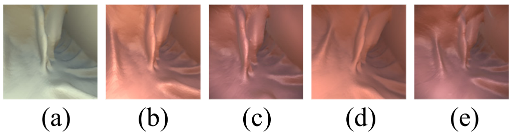

Figure 7: (a) query image, (b), (c), (d), and (e) retrieved images based on Resnet50 based method.

Table 5 shows F1 scores for Case 5 (DS-MiDas-D2) through Case 12 (R50-RGB-D2), and indicates the proposed feature-based method outperforms the Resnet50 feature-based method for all different image sets from Dataset2. As seen in Table 5, the proposed method achieves around 86.9 ~ 92.8 % of accuracy on the depth maps by MiDas for Dataset2, which indicates that our proposed method is promising for practical use. As seen in Cases 5 (DS-MiDas-D2), 7 (DS-DenseNet-D2), and 9 (DS-Pix2pix-D2) in Table 5, the depth maps generated by MiDas provided much better accuracies. The reason is that Pix2pix and DenseNet-169 trained using Dataset1 were applied to Dataset2, so they did not generate accurate depth maps.

Table 5: Two methods and their accuracies of four different retrievals on Dataset2.

Experiment	Top1	Top2	Top3	Top4
Case 5 (DS-MiDas-D2)	0.928	0.925	0.907	0.869
Case 6 (R50-MiDas-D2	0.386	0.318	0.269	0.243
Case 7 (DS-DenseNet-D2)	0.135	0.139	0.114	0.107
Case 8 (R50-DenseNet-D2)	0.107	0.096	0.090	0.086
Case 9 (DS-Pix2pix-D2)	0.121	0.143	0.131	0.127
Case 10 (R50-Pix2pix-D2)	0.093	0.103	0.095	0.082
Case 11 (DS-RGB-D2)	0.143	0.114	0.114	0.100
Case 12 (R50-RGB-D2)	0.114	0.104	0.093	0.086

Figure 8 shows an example of query and retrieval in which Figure 8(a) is a query image in Dataset2, and Figure 8(b), (c), (d) and (e) are retrieved images using the proposed method. They are all very similar in terms of surface topology regardless of their colors.

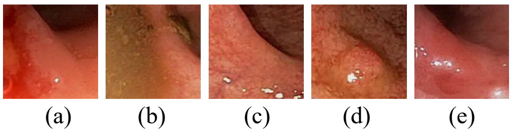
(a) (b) (c) (d) (e)

Figure 8: (a) query image, (b), (c), (d), and (e) retrieved images based on the proposed method.

Figure 9 shows an example of query and retrieval in which Figure 9(a) is a query image (same image in Figure 8 (a)), and Figure 9(b), (c), (d) and (e) are retrieved images using Resnet50 based method. All retrieved images are not very similar in terms of surface topology.

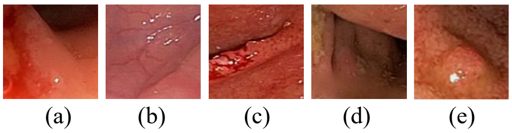
(a) (b) (c) (d) (e)

Figure 9: (a) query image, (b), (c), (d), and (e) retrieved images based on the Resnet50 based method.

We compared four distance functions (Equation (5), Equations (10), (11) and (12)) discussed in Section 3.2, and their results are in Table 6. Table 6 shows Cases 1 (DS-Dep-D1) and 5 (DS-MiDas-D2) in which the proposed method was applied to the ground truth depth maps in Dataset1, and the depth maps by MiDas for Dataset2. The F1-scores in Table 6 are the results of Top1 query where a most similar single image is retrieved. As seen in table 6, Equation (5) provided a best result among them.

Table 6: Comparison of four distance functions and their F1-scores.

Experiment	Eq. (5)	Eq. (10)	Eq. (11)	Eq. (12)
Case1 (DS-Dep-D1)	0.925	0.925	0.380	0.130
Case5 (DS-MiDas-D2)	0.928	0.907	0.579	0.421

5 CONCLUDING REMARK AND FUTURE WORK

This paper presents a new technique to compare images in which low-level visual features (i.e., color, shape, texture, and spatial layout) or Convolutional Neural Network features are not effective. This new technique finds image similarity in terms of the surface topology using the depth map images. The experiments based on synthetic and real colonoscopy images show that the proposed technique achieves around 90% accuracy, indicating it can potentially be used in practice. In the future, to improve the accuracy of the proposed method, we will consider an enhancement of the depth map generation methods discussed in Section 3.1, and investigate a different method (i.e., Jensen–Shannon divergence (Frank Nielsen, 2021)) of measuring the similarity between two lines as discussed in Section 3.2.

ACKNOWLEDGEMENTS

For MiDas, we used the code from the web page (https://github.com/isl-org/dpt), under MIT license. For Pix2pix, we used the code from TensorFlow GitHubpage (https://www.tensorflow.org/tutorials/generative/Pix2pix) under Apache license version V2.0. For DenseNet-169, we used code from the webpage (https://github.com/ialhashim/DenseDepth) under GNU General Public License v3.0. All those three types of licenses are in the permissive category and free to use for individual. For the synthetic data (Dataset1 in Table1) we acknowledge (Rau et al., 2019) for the synthetic dataset based on the condition to cite their study paper.

REFERENCES

Meenalochini, M., Saranya, K., Rajkumar, G. V., & Mahto, A. (2018, October). Perceptual hashing for content based image retrieval. In *2018 3rd International Conference on Communication and Electronics Systems (ICCES)* (pp. 235-238). IEEE.

Öztürk, Ş. (2021). Class-driven content-based medical image retrieval using hash codes of deep features. *Biomedical Signal Processing and Control*, *68*, 102601.

Chen, W., Liu, Y., Wang, W., Bakker, E., Georgiou, T., Fieguth, P., Liu, L., & Lew, M. S. (2021). *Deep Learning for Instance Retrieval: A Survey*. https://doi.org/10.48550/arxiv.2101.11282

Latif, A., Rasheed, A., Sajid, U., Ahmed, J., Ali, N., Ratyal, N. I., ... & Khalil, T. (2019). Content-based image retrieval and feature extraction: a comprehensive review. *Mathematical Problems in Engineering*, *2019*.

Mokter, M.F., Idris , Azeez Idris., Oh, J., Tavanapong, W., Wong, J., & Groen, P. C. D. (2022, October). Severity Classification of Ulcerative Colitis in Colonosco-py Videos by Learning from Confusion. In *17th International Symposium on Visual Computing*. Springer, Cham.

Rahman, M. M., Oh, J., Tavanapong, W., Wong, J., & Groen, P. C. D. (2021, October). Automated Bite-block Detection to Distinguish Colonoscopy from Upper Endoscopy Using Deep Learning. In *International Symposium on Visual Computing* (pp. 216-228). Springer, Cham.

Mokter, M. F., Oh, J., Tavanapong, W., Wong, J., & Groen, P. C. D. (2020, October). Classification of ulcerative colitis severity in colonoscopy videos using vascular pattern detection. In *International Workshop on Machine Learning in Medical Imaging* (pp. 552-562). Springer, Cham.

Tejaswini, S. V. L. L., Mittal, B., Oh, J., Tavanapong, W., Wong, J., & Groen, P. C. D. (2019, October). Enhanced approach for classification of ulcerative colitis severity in colonoscopy videos using CNN. In *International Symposium on Visual Computing* (pp. 25-37). Springer, Cham.

Willmott, C. J., & Matsuura, K. (2005). Advantages of the mean absolute error (MAE) over the root mean square error (RMSE) in assessing average model performance. *Climate research*, *30*(1), 79-82.

Ranftl, R., Bochkovskiy, A., & Koltun, V. (2021). Vision transformers for dense prediction. In *Proceedings of the IEEE/CVF International Conference on Computer Vision* (pp. 12179-12188).

Ranftl, R., Lasinger, K., Hafner, D., Schindler, K., & Koltun, V. (2020). Towards robust monocular depth estimation: Mixing datasets for zero-shot cross-dataset transfer. *IEEE transactions on pattern analysis and machine intelligence*.

Rau, A., Edwards, P. J., Ahmad, O. F., Riordan, P., Janatka, M., Lovat, L. B., & Stoyanov, D. (2019). Implicit domain adaptation with conditional generative adversarial networks for depth prediction in endoscopy. *International journal of computer assisted radiology and surgery*, *14*(7), 1167-1176.

Li, Z., & Snavely, N. (2018). Megadepth: Learning single-view depth prediction from internet photos. In *Proceedings of the IEEE conference on computer vision and pattern recognition* (pp. 2041-2050).

Isola, P., Zhu, J. Y., Zhou, T., & Efros, A. A. (2017). Image-to-image translation with conditional adversarial networks. In *Proceedings of the IEEE conference on computer vision and pattern recognition* (pp. 1125-1134).

Alhashim, I., & Wonka, P. (2018). High quality monocular depth estimation via transfer learning. *arXiv preprint arXiv:1812.11941*.

Laina, I., Rupprecht, C., Belagiannis, V., Tombari, F., & Navab, N. (2016, October). Deeper depth prediction with fully convolutional residual networks. In *2016 Fourth international conference on 3D vision (3DV)* (pp. 239-248). IEEE.

Fu, H., Gong, M., Wang, C., Batmanghelich, K., & Tao, D. (2018). Deep ordinal regression network for monocular depth estimation. In *Proceedings of the IEEE conference on computer vision and pattern recognition* (pp. 2002-2011).

He, K., Zhang, X., Ren, S., & Sun, J. (2016). Deep residual learning for image recognition. In *Proceedings of the IEEE conference on computer vision and pattern recognition* (pp. 770-778).

Alsmadi, M. K. (2017). An efficient similarity measure for content based image retrieval using memetic algorithm. *Egyptian journal of basic and applied sciences*, *4*(2), 112-122.

Frank Nielsen (2021). "On a variational definition for the Jensen-Shannon symmetrization of distances based on the information radius". Entropy. MDPI. 23 (4): 464. doi:10.3390/e21050485. PMID 33267199.